Unusual ground states via monotonic convex pair potentials

É. Marcotte,[1] F. H. Stillinger,[2] and S. Torquato[1,2,3,4,5,a)]
[1]*Department of Physics, Princeton University, Princeton, New Jersey 08544, USA*
[2]*Department of Chemistry, Princeton University, Princeton, New Jersey 08544, USA*
[3]*Princeton Center for Theoretical Science, Princeton University, Princeton, New Jersey 08544, USA*
[4]*Princeton Institute for the Science and Technology of Materials, Princeton University, Princeton, New Jersey 08544, USA*
[5]*Program in Applied and Computational Mathematics, Princeton University, Princeton, New Jersey 08544, USA*

(Received 13 January 2011; accepted 22 March 2011; published online 27 April 2011)

We have previously shown that inverse statistical-mechanical techniques allow the determination of optimized isotropic pair interactions that self-assemble into low-coordinated crystal configurations in the d-dimensional Euclidean space $\mathbb{R}^d$. In some of these studies, pair interactions with multiple extrema were optimized. In the present work, we attempt to find pair potentials that might be easier to realize experimentally by requiring them to be monotonic and convex. Encoding information in monotonic convex potentials to yield low-coordinated ground-state configurations in Euclidean spaces is highly nontrivial. We adapt a linear programming method and apply it to optimize two repulsive monotonic convex pair potentials, whose classical ground states are counterintuitively the square and honeycomb crystals in $\mathbb{R}^2$. We demonstrate that our optimized pair potentials belong to two wide classes of monotonic convex potentials whose ground states are also the square and honeycomb crystal. We show that these unexpected ground states are stable over a nonzero number density range by checking their (i) phonon spectra, (ii) defect energies and (iii) self assembly by numerically annealing liquid-state configurations to their zero-temperature ground states. © *2011 American Institute of Physics*. [doi:10.1063/1.3576141]

I. INTRODUCTION

The study of particle self-assembly has been an ongoing area of research since Whitesides[1] coined the term two decades ago. Self-assembly is defined as the spontaneous organization of particles, be they atoms, molecules or supramolecules, into a given many-particle configuration. This organization occurs without any external force through noncovalent interaction between the particles. Naturally occurring examples include the formation of DNA double helices, lipid bilayers, and ionic crystals.

There are two main methods one can take to design self-assembling systems: the forward and the inverse approaches. The forward approach begins with a many-particle system with specified interactions, and obtains the stable many-particle configuration. This approach, used both computationally and experimentally, has led to the discovery of a wide variety of novel many-particle configurations,[2–9] but is not best suited to find new many-particle configurations with targeted properties. To do this, it is necessary to use the inverse approach, which attempts to find the optimal interactions that yield a targeted many-particle configuration with desirable bulk physical properties.

This work continues our program on using inverse approaches to optimize pair interactions to achieve novel targeted ground-state configurations in d-dimensional Euclidean space $\mathbb{R}^d$. Previous investigations reported optimized pair interactions that stabilize low-coordinated crystals as ground states, including the square and honeycomb crystals[10] in $\mathbb{R}^2$ and simple cubic[11] and diamond[12] crystals in $\mathbb{R}^3$, materials with negative thermal expansion, and[13] negative Poisson's ratio.[14] Moreover, potentials possessing disordered ground states[15,16] have been produced with novel optical properties.[16,17] We envision using colloids and/or polymers to realize such designed potentials because it is possible to manipulate and control their interactions.[6,18–20]

Earlier uses of the inverse approach[10] did not regard experimental feasibility as a constraint. These investigations allowed a largely unconstrained class of spherically symmetric pair potentials. In some of these instances, multiple potential wells were utilized to achieve the desired target configurations,[10,12] which may be difficult to realize experimentally. Our objective in the present study is to stabilize low-coordinated crystal configurations in Euclidean space, restricting ourselves to a class of monotonically decreasing pair potentials, which are relatively easy to produce experimentally. However, encoding information in monotonic potentials to yield low-coordinated ground-state configurations in Euclidean space is nontrivial. These potentials must not only successfully discriminate against close-packed (highly coordinated) crystal configurations but also the infinitesimally close configurations obtained by slightly deforming the target crystal. In addition, both of these theoretical challenges are further complicated by the monotonicity constraint.

We are motivated by the work of Cohn and Kumar,[21] who have rigorously constructed potentials that stabilize unusual targeted configurations on the surface of a d-dimensional sphere using only monotonic convex pair potentials. A crucial

a)Author to whom correspondence should be addressed. Electronic mail: torquato@princeton.edu.

difference between the work of Ref. 21 and this study is that we consider noncompact (infinite) Euclidean spaces. The fact that Cohn and Kumar restricted themselves to compact spaces made their problem comparatively easy to solve because their pair potentials had compact support set by the sphere radius. A consequence of using repulsive monotonic potentials is that such systems are required to be under positive pressure, a condition that is easily enforceable experimentally.

In this paper, we specifically use the inverse approach to obtain repulsive monotonic convex potentials whose ground states in $\mathbb{R}^2$ are either the square lattice or the honeycomb crystal. Thus, our work is a theoretical proof of concept that monotonic convex potentials can counterintuitively stabilize low-coordinated two-dimensional crystals. A summary of preliminary results is available,[22] but in this paper we present a detailed explanation of our numerical methods, a complete analysis of the stability of the resulting crystalline ground states, and a thorough demonstration of how monotonic convex potentials can stabilize the studied unusual ground states. To better explain the characteristic features of the optimized potentials, we introduce a new measure, the *generalized coordination functions*, which to our knowledge have not been previously used. We show the utility of these functions to enable the stabilization of the square and honeycomb crystals via a large family of potential functions.

This paper is organized as follows: Sec. II is devoted to a technical explanation of how the new potentials are devised. Section III presents the family of monotonic convex potentials that we use and analyzes their energetic and mechanical-stability properties for the square and honeycomb crystal ground states. We also relax the convexity condition to see whether the square lattice can still be produced as a ground-state configuration. Finally, Sec. IV summarizes the impacts of these new results and speculates on how they could be extended.

II. THEORY

A. Background

1. Pair potentials

We consider a system of N particles, with positions $\mathbf{r}_1$, $\mathbf{r}_2$, ..., $\mathbf{r}_N$ in a volume V contained in $\mathbb{R}^d$. In the absence of an external field, the potential energy of the system $\Phi_N(\mathbf{r}^N)$ is a function of the particle positions:

$$\Phi_N(\mathbf{r}^N) = \sum_{i<j} v_2(\mathbf{r}_i, \mathbf{r}_j) + \sum_{i<j<k} v_3(\mathbf{r}_i, \mathbf{r}_j, \mathbf{r}_k) + \cdots, \qquad (1)$$

where the v_n are the intrinsic n-particle potentials. Our focus is on those cases in which only the pair potential v_2 is present and where it is also isotropic (i.e., a radial function): $v_2(\mathbf{r}_i, \mathbf{r}_j) \equiv v(r_{ij})$, with $r_{ij} = |\mathbf{r}_i - \mathbf{r}_j|$. This reduces the total potential expression to

$$\Phi_N(\mathbf{r}^N) = \sum_{i<j} v(r_{ij}). \qquad (2)$$

We recognize that systems encountered in the laboratory typically exhibit some nonpairwise contributions, but we defer for later study how these contributions could be minimized by selection of the specific systems for analysis and what their residual effects would be.

If the number density $\rho = N/V$ is kept constant, Φ_N is asymptotically proportional to N, so it is useful to define a normalized energy value using their ratio. In this paper, a key quantity that we will consider is twice the energy per particle, i.e.,

$$u = 2\Phi_N/N. \qquad (3)$$

2. Finding the classical ground state

For a system with a given number of particles N in some volume V and with a potential energy function $\Phi_N(\mathbf{r}^N)$, the classical ground state is defined as the configuration set of the particle positions $\mathbf{r}^N$ with the globally minimal potential energy. To find the putative targeted ground states, we use the well-known simulated annealing method.[10] We begin with an initial configuration of N particles chosen from a Poisson point process in a box of volume V with periodic boundary conditions. Initially, a large temperature T is selected and the particles are moved according to the Metropolis Monte Carlo algorithm. The temperature T is then gradually reduced to zero. If this procedure is done slowly enough, the resulting configuration is likely the ground state. To improve the efficiency of our method, we use a steepest–descent method to relax the particles at the end of the simulated annealing. Furthermore, since simulated annealing calculations often tend to become trapped in deep local minima, we repeat this process many times, only keeping the final configuration with the lowest potential energy.

B. Methodology

1. Functional form

To simplify the notation, let us define a configuration C as a set of particle positions $\mathbf{r}_1, \mathbf{r}_2, \ldots$ in $\mathbb{R}^d$. A configuration defined in this sense is perfectly general, incorporating both periodic as well as disordered point processes.

Let us assume that a certain pair potential v has the target configuration C^* as its ground state. Thus, we have

$$u(v, C^*) \le u(v, C) \qquad \forall C, \qquad (4)$$

where u is defined by relation (3). Intuitively, it should be possible to find a valid potential v by expressing it in terms of a list of M parameters $a_1, \ldots, a_M$ and varying the parameters until inequality (4) is satisfied for all possible configurations:

$$v \equiv v(a_1, \ldots, a_M). \qquad (5)$$

Since checking all possible configurations is impossible (because there is an uncountably infinite number of them), we restrict ourselves to a subset, which we call the "competitor" configurations $\mathbf{C}$. In this way, we can redefine the problem as an optimization,[10] where we seek to maximize the energy difference between the targeted configuration C^* and its closest competitor configurations. To do so, we introduce Δ, a utility variable which is maximized while constrained by

$$u\big(v(a_1, \ldots, a_M), C^*\big) \le u\big(v(a_1, \ldots, a_M), C\big) - \Delta \quad \forall C \in \mathbf{C}. \qquad (6)$$

For a given potential v, Δ can be as large as the smallest energy difference, $u(v, C) - u(v, C^*)$, between a competitor and the targeted configurations. Therefore, allowing v to vary the optimization procedure enables us to find the potential that maximizes the energy difference between the target configuration and its closest competitor.

In the case where we do not want all competitors to be treated on an equal footing and seek to prioritize some of them, we can add a modulating factor $m(C)$ to the inequality:

$$u\big(v(a_1, \ldots, a_M), C^*\big) \leq u\big(v(a_1, \ldots, a_M), C\big) - m(C)\Delta \forall C \in \mathbf{C}. \quad (7)$$

One particularly useful property of the modulating factor is that it can be chosen to be very small for configurations close to C^*. Even the limiting case $C^* \in \mathbf{C}$ can be considered if $m(C^*) = 0$ is enforced.

2. Potential form

For inequality (7) to be usable, $v(\{a_i\})$, C, and $m(S)$ must be defined. The first choice to be made is the form of the pair potential function $v(\{a_i\})$. Since inequality (7) is linear with respect to twice the energies per particle $u(v, C)$, and the $u(v, C)$ are linear in terms of the pair potential $v(\{a_i\})$ for each configuration C, making the pair potential linear in the parameters $\{a_i\}$ ensures the overall linearity of the system:

$$v(r) = \sum_{i=1}^{M} a_i f_i(r), \quad (8)$$

$$\Phi(v, C) = \sum_{j<k} \sum_{i=1}^{M} a_i f_i(r_{jk}) = \sum_{i=1}^{M} a_i \left[\sum_{j<k} f_i(r_{jk}) \right]. \quad (9)$$

This simplifies the optimization problem, since it allows one to use many of the standard linear programming methods to determine the optimal parameters, such as the simplex algorithm. Another advantage of using a linear form for the pair potential is apparent from Eq. (9): we need only to sum over all particle pairs once for a given configuration, greatly reducing the computational cost. It bears mentioning that the sums over j and k are over *all* particles of the configuration, making them infinite in the large system limit. However, if the configuration is periodic, by using u instead of Φ, the normalized sum reverts to a bounded lattice sum.

For this paper, the $f_i(r)$ are taken to be negative powers of r, with a common cutoff at some distance $R > 0$:

$$v(r) \equiv \begin{cases} \sum_{i=1}^{M} \frac{a_i}{r^i} & r \leq R, \\ 0 & r > R. \end{cases} \quad (10)$$

Since we not only desire to have both the pair potential $v(r)$ and the corresponding force $-dv/dr$ be continuous, but need also to be able to calculate phonon spectra, we require $v(r)$ and both its first and second derivatives to be continuous at $r = R$. This is equivalent to adding the following constraints:

$$\sum_{i=1}^{M} \frac{a_i}{R^i} = 0, \quad \sum_{i=1}^{M} \frac{i a_i}{R^{i+1}} = 0, \quad \sum_{i=1}^{M} \frac{i(i+1) a_i}{R^{i+2}} = 0. \quad (11)$$

The rationale for using the functions from Eq. (10) is that they can accurately reproduce most other functions since they become Taylor series in terms of $1/r$ as M and R grow larger. Additionally, they can naturally reproduce a quasi-hard-core repulsion: $\lim_{r \to 0^+} v(r) = \infty$, as long as $a_M > 0$. Other potentials have been tried, such as those involving positive powers of r, but numerical experiments show that they are less stable and more affected by numerical imprecisions, particularly with longer cutoffs.

It is easy to see from Eq. (7) that multiplying all of the a_i by some positive constant amounts to multiplying the objective Δ by the same constant. From there, it is clear that the problem as written is not bounded, and that if it is possible to obtain a solution for which Δ is greater than zero, then solutions exist for any positive Δ, including arbitrarily large values. To impose a scale, we fix the value of the potential at the nearest-neighbor distance of the target configuration as unity, which leads to the following constraint:

$$v(r = 1) = \sum_{i=1}^{M} a_i = 1. \quad (12)$$

Additionally, the a_i are all constrained to be in the $[-1000, +1000]$ range, since the problem still is not totally bounded after fixing $v(r = 1)$.

While previous papers[10–12] have succeeded in obtaining pair potentials resulting in specific crystal ground-state configurations, their functions use extrema (minima and maxima) to either favor or disfavor certain nearest neighbor distances. Doing so may allow the determination of pair potentials with the desired classical ground state, but at the same time, leads to potentials that may not be experimentally realizable. In an attempt to find potentials that are more experimentally feasible, two additional constraints have been added: $v(r)$ must be both monotonically decreasing [for all $r' > r$, $v(r') \leq v(r)$] and convex [for all r, r' and $b \in [0, 1]$, $v(br + (1-b)r') \leq bv(r) + (1-b)v(r')$]. For our potential form, these conditions can be written as

$$-\frac{dv}{dr} = \sum_{i=1}^{M} \frac{i a_i}{r^{i+1}} \geq 0 \quad \forall r < R, \quad (13)$$

$$\frac{d^2 v}{dr^2} = \sum_{i=1}^{M} \frac{i(i+1) a_i}{r^{i+2}} \geq 0 \quad \forall r < R. \quad (14)$$

Inequalities (13) and (14) are both linear. However, they introduce a condition for every possible value of r. To avoid the numerical impossibility of dealing with an infinite number of

conditions, we restrict ourselves to a large, but finite, number of values of r at which we enforce the conditions.

3. Competitors

Once the functional form is chosen, the competitor set $\mathbf{C}$ and modulation $m(C)$ still have to be selected. Since a well chosen $\mathbf{C}$ is sufficient to either find, or disprove, the existence of a potential with the desired ground state, here we restrict ourselves to a constant $m(C) = 1$ modulation. However, such a choice puts all competitors on an equal footing, which often results in potentials that do not discriminate against distinctly different configurations.

The method employed to specify $\mathbf{C}$ is to start with it containing only a single competitor (typically the triangular lattice) and to create a trial potential v_1 from that initial $\mathbf{C}$, as described in Sec. II B 1. After calculating the trial potential ground state C_1, its energy with the trial potential is compared with that of the targeted configuration C^*. If the energy of C_1 is lower than that of C^*, the trial potential is incorrect, so we add C_1 to the set of competitors and repeat the process with a new trial potential v_2. Otherwise, the ground state of the trial potential is the target configuration and the trial potential is the desired potential.[23]

Our method is an adaptation of the one presented by Cohn and Kumar.[21] It was modified to use simulated annealing instead of a gradient descent method to find the ground states of the trial potentials due to the typically numerous local minima of the $\Phi_N(\mathbf{r}^N)$ energy landscape, which makes it almost impossible to find the ground state by simply using a gradient descent technique. A second difference is that we only add configurations to the set of competitors if they have a lower energy than the target for the current trial potential. Adding all of the obtained configurations was found to be highly unstable because imperfect energy minimizations led to adding configurations close to the target, causing inequality (7) to only consider close competitors.

Eventually, this algorithm will, in principle, find an optimal potential v^*, or prove that no such potential exists with the functional form used. But to do so, an infinite number of iterations can be required, since over time it fills $\mathbf{C}$ with all possible configurations but C^* reverting slowly to inequality (4). In practice, this is not necessary. For most, but not all, of the studied target configurations in two-dimensions having only the triangular lattice as a competitor is enough to find an optimal potential.

C. Generalized coordination functions

For isotropic pair potentials, the list of the neighbor separations and their multiplicities is a crucial piece of information for understanding which configurations are energetically favorable. However, while this list is useful when dealing with pair potentials that have well-defined minima or maxima, it does not convey much information for strongly constrained pair potentials, such as the monotonic convex potentials considered in this paper. Therefore, we introduce *generalized coordination functions*, a new measure that amplifies the differences between configurations that are relevant to the restricted potentials. This is preferred, especially if such differences can be correlated to the features of the potentials. Of particular interest are the *coordination functions of order n*, which apply to potentials that have nth order derivatives restricted to either being non-negative or non-positive (depending on the parity of n).

Writing u, twice the energy per particle [cf. Eq. (3)], in terms of the set of particle positions C, we get

$$u = \frac{1}{N} \sum_{\mathbf{p}\neq\mathbf{q}\in C} v(|\mathbf{p}-\mathbf{q}|). \tag{15}$$

By replacing the sum with an integral using delta functions, we now have a function that describes the radial distribution of the neighbors,

$$\begin{aligned} u &= \int_{r=0}^{\infty} dr\, v(r) \left[\frac{1}{N} \sum_{\mathbf{p}\neq\mathbf{q}\in C} \delta(r - |\mathbf{p}-\mathbf{q}|) \right] \\ &= \int_{r=0}^{\infty} dr\, v(r) \mathcal{Z}_0(r), \end{aligned} \tag{16}$$

where $\mathcal{Z}_0(r)$ is the coordination function of order 0, defined as

$$\mathcal{Z}_0(r) \equiv \frac{1}{N} \sum_{\mathbf{p}\neq\mathbf{q}\in C} \delta(r - |\mathbf{p}-\mathbf{q}|). \tag{17}$$

Assuming that $\mathcal{Z}_0(r)$ is zero at $r = 0$, and that $v(r)$ and all its derivatives go to zero as r goes to infinity, we can use integration by parts to write u as a function of the derivatives of $v(r)$. Let us first define the coordination function of order n, $\mathcal{Z}_n(r)$, recursively:

$$\mathcal{Z}_{n+1}(r) \equiv \int_{r'=0}^{r} dr' \mathcal{Z}_n(r'). \tag{18}$$

Then, we have

$$u = \int_{r=0}^{\infty} dr\, v(r) \mathcal{Z}_0(r) \tag{19}$$

$$= (v(r)\mathcal{Z}_1(r))_{r=0}^{\infty} - \int_{r=0}^{\infty} dr \frac{dv}{dr} \mathcal{Z}_1(r) \tag{20}$$

$$= -\int_{r=0}^{\infty} dr \frac{dv}{dr} \mathcal{Z}_1(r). \tag{21}$$

The integration by parts can be repeated as many times as $v(r)$ is differentiable:

$$u = (-1)^n \int_{r=0}^{\infty} dr \frac{d^n v}{dr^n} \mathcal{Z}_n(r). \tag{22}$$

Equation (22) is particularly relevant when we restrict ourselves to pair potentials with constrained derivatives. As an example, if we know that for two distinct configurations A and B that $\mathcal{Z}_2^A(r) < \mathcal{Z}_2^B(r)$ for all values of r, then the configuration A will always have a lower energy than the

configuration B in the presence of a convex pair potential. Hence, no such potential will have the configuration B as a ground state.

The $\mathcal{Z}_n(r)$ functions can be generalized to yield information for any problem where it is possible for the pair potential to be expressed as a linear combination of a family of functions $f(r,s)$: $v(r) = \int_s ds c(s) f(r,s)$, especially when the coefficients $c(s)$ are restricted to be non-negative:

$$u = \int_{r=0}^{\infty} dr v(r) \mathcal{Z}_0(r) \tag{23}$$

$$= \int_{r=0}^{\infty} dr \int_s ds c(s) f(r,s) \mathcal{Z}_0(r) \tag{24}$$

$$= \int_s ds c(s) \int_{r=0}^{\infty} dr f(r,s) \mathcal{Z}_0(r) \tag{25}$$

$$= \int_s ds c(s) \widetilde{\mathcal{Z}}_f(s). \tag{26}$$

Here $\widetilde{\mathcal{Z}}_f(s)$ (the subscript f denoting a family of functions) is defined as

$$\widetilde{\mathcal{Z}}_f(s) \equiv \int_{r=0}^{\infty} dr f(r,s) \mathcal{Z}_0(r). \tag{27}$$

Equation (22) can be obtained from Eq. (26) by using $c(s) = (-1)^n \frac{d^n v}{dr^n}(r=s)$ and $f(r,s) = \Theta(s-r)(s-r)^{n-1}/(n-1)!$.

III. RESULTS

The method presented in Sec. II B is applied to two target configurations in two-dimensions: the square and honeycomb crystals. The obtained optimized pair potentials and their properties are presented in Secs. III A and III B, respectively.

A. Square lattice

Consider a square lattice with a nearest neighbor distance of unity as the target configuration. We restrict our optimization to monotonic convex pair potentials with a cutoff of $R = 2$. The simulated-annealing optimization method results in the following pair potential:

$$v(r) = \begin{cases} \left(\dfrac{28.424}{r} - \dfrac{245.756}{r^2} + \dfrac{786.742}{r^3} \right. \\ \quad - \dfrac{1000}{r^4} - \dfrac{24.043}{r^5} + \dfrac{1000}{r^6} \\ \quad - \dfrac{47.967}{r^7} - \dfrac{1000}{r^8} + \dfrac{64.527}{r^9} \\ \quad \left. + \dfrac{1000}{r^{10}} - \dfrac{712.166}{r^{11}} + \dfrac{151.240}{r^{12}} \right) & r \le 2 \\ 0 & r > 2 \end{cases} . \tag{28}$$

This function is plotted in Fig. 1. The choice of $M = 12$ terms in our potential is a compromise between using many terms to strongly discriminate against competitors and using few terms to avoid numerical instabilities. Potential (28) is an illustrative example from an infinite class of monotonic convex pair potentials that have the square lattice as their ground state.

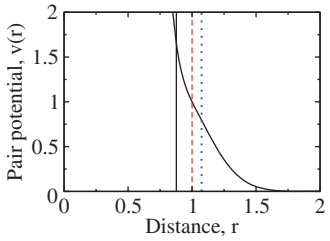

FIG. 1. Optimized monotonic convex pair potential from Eq. (28) targeting the square lattice at unit number density. The three vertical lines represent the nearest-neighbor distances for the honeycomb crystal (black solid), the square lattice (red dashed), and the triangular lattice (blue dotted) at the same number density. The value of $v(r)$ at these distances is 1.6542, 1 and 0.7937, respectively

To confirm that the ground state of potential (28) is indeed the square lattice configuration, we performed simulated annealing calculations. The result of these calculations is shown in Fig. 2. Examining many different simulated-annealing solutions, no other configuration is of lower energy than the square lattice. Of the four slowest simulated annealing calculations performed, three of them reach the target ground state. In the remaining case, the particles align in a square lattice, but do not align correctly within the periodic simulation box, resulting in a line defect where the lattice meets its periodic image. As with all other calculations (with more rapid annealing) that did not reach the perfect square-lattice configuration, the imperfect lattice total energy is higher than that for the perfect square lattice.

Simulated annealing calculations are also conducted on systems where the central cell shape is not kept constant. Even if the central cell is allowed to deform to any parallelogram of constant area, no configuration is found to be of lower energy than the square lattice. This strengthens our confidence that the square lattice is indeed the ground state for potential (28).

1. Discrimination against other crystals

Since we are using a pair potential with a short-ranged cutoff, the value of twice the energy per particle u only depends on the first few coordination shells. At unit density, we

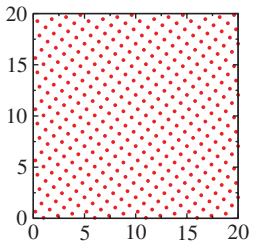

FIG. 2. Ground state of the potential (28) with 400 particles in a 20×20 box with periodic boundary conditions as obtained by slowly annealing the system starting from a fluid. For illustration purposes, the point particles are shown to have finite sizes. This rotated square lattice has the same u as would a square lattice aligned with the box boundaries.

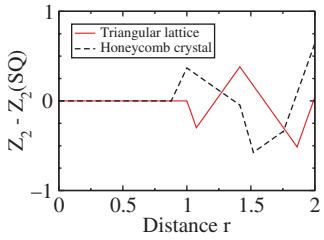

FIG. 3. Differences between the coordination functions of second order $\mathcal{Z}_2$ of the triangular lattice and the honeycomb crystal and the square lattice. All three lattices have a number density of unity.

can explicitly write u for the square, triangular, and honeycomb crystals:

$$u_{\mathrm{SQ}} = 4v(r=1) + 4v(r=1.414) = 4.4556, \tag{29}$$

$$u_{\mathrm{TR}} = 6v(r=1.075) + 6v(r=1.861) = 4.7635, \tag{30}$$

$$u_{\mathrm{HC}} = 3v(r=0.877) + 6v(r=1.520) + 3v(r=1.755) = 5.2363. \tag{31}$$

Furthermore, as can be seen in Fig. 1, potential (28) decreases very quickly, being equal to only 0.1139 at the square lattice second neighbor ($r = 1.414$). Therefore, examining only the nearest neighbors provides insight on why potential (28) succeeds at stabilizing the square-lattice configuration. While the potential is definitely higher for the square-lattice nearest neighbors [$v(r=1)=1$] than for the triangular-lattice nearest neighbors [$v(r=1.075)=0.7937$], its coordination number is smaller (four compared to six), and hence its total energy is the lowest. The same argument does not hold for the honeycomb crystal, since it has only three nearest neighbors. A much higher associated energy [$v(r=0.877)=1.6542$] prevents the honeycomb crystal from having a lower total energy than the square lattice.

While looking at the occupancy numbers of the successive coordination shells and the associated interactions of these shells aids our understanding of why potential (28) stabilizes the square lattice, it does not explain how such a monotonic convex potential can exist. However, the differences between the coordination functions of second order $\mathcal{Z}_2$ of the square lattice and the triangular and honeycomb crystals (Fig. 3) illustrate the necessary features for a monotonic convex potential to favor the square lattice over the triangular or honeycomb crystals. First, discriminating against the honeycomb crystal is easy, as its $\mathcal{Z}_2$ is larger than the square $\mathcal{Z}_2$ near $r = 1$. Therefore, a potential with a very large second derivative for values of r close to 1 will strongly discriminate against the honeycomb crystal. Second, there is a range of values of r where both the triangular and the honeycomb crystals' $\mathcal{Z}_2$'s are larger than that of for the square lattice, specifically from $r \sim 1.2$ to $r \sim 1.4$. So a potential with a large second derivative in that range will favor the square lattice. Third, the triangular lattice $\mathcal{Z}_2$ is smaller around $r \sim 1.1$ and $r \sim 1.8$. Thus the second derivative must be close to zero at these points. Finally, the differences between the $\mathcal{Z}_2$'s become quite chaotic for larger values of r (not shown here), something which worsens if more competing configurations are considered. Consequently, there is no advantage in increasing the cutoff R to larger values. As can be seen in Fig. 4, the pair potential function (28) possesses all of these features, which explains how it succeeds in having the square lattice as its ground state.

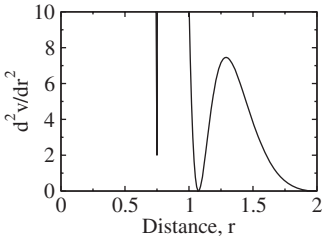

FIG. 4. Second derivative of the pair potential d^2v/dr^2 from Eq. (28) versus the distance r.

As a test to see if $\mathcal{Z}_2$ can be used to design a monotonic convex potential, we build a piecewise-polynomial potential using only information from the $\mathcal{Z}_2$ analysis,

$$v(r) = \begin{cases} 5r^2 - 10.45r + 5.61875 & r \le 1, \\ -0.45r + 0.61875 & 1 < r \le 1.15, \\ 0.5r^2 - 1.6r + 1.28 & 1.15 < r \le 1.6, \\ 0 & 1.6 < r, \end{cases} \tag{32}$$

which has a second derivative of

$$\frac{d^2v}{dr^2} = \begin{cases} 10 & r \le 1, \\ 0 & 1 < r \le 1.15, \\ 1 & 1.15 < r \le 1.6, \\ 0 & 1.6 < r. \end{cases} \tag{33}$$

Simulated annealing simulations confirm that this potential has the square lattice as its ground state, which proves that the precise form of the potential (28) is not necessary to have the square lattice as a ground state, however, potential (32) is flawed, as its second derivative is not continuous at the first neighbor distance ($r = 1$) preventing its phonon spectrum from being calculated. Furthermore, since potential (32)'s second derivative is exactly zero for r's slightly larger than 1, at lower densities the square lattice will not be the ground state; it is replaced by a rectangular lattice. Nevertheless, potential (32) proves that it is possible to construct a potential that stabilizes the square lattice using only information from the generalized coordination functions. Furthermore, since such requirements are relatively nonrestrictive, there is still a large class of potentials that stabilize the square lattice, one of which is potential function (32).

2. Stability

There are three basic criteria which impact whether the configurations created using the proposed potential are stable square lattices: their response to changes in the number density, their phonon stability and their response to slight modifications in the potential. This last criterion is not

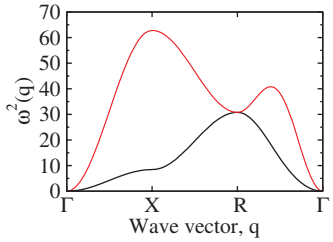

FIG. 5. Phonon spectrum for the potential function (28) on a square lattice with unit nearest neighbor distance ($\rho = 1$). Only a representative subset of wave vectors is presented here, but all the wave vectors have been tested to confirm that no mode is unstable.

formally studied here, due to the difficulty of modifying the value of a polynomial only over a short range. However, as shown in Sec. III A 1, as long as the second derivative of the modified potential displays the features described therein, the modified potential will maintain a square-lattice ground state.

Figure 5 shows the squared frequency of the different phonon modes for the square lattice as a function of their wave vectors. For any wave vector, if one of the modes has a negative squared frequency, then the resulting imaginary frequency mode is unstable, a sign that the square lattice is not a local minimum in the energy landscape. Since none of the mode squared frequencies are negative for any wave vector, the square lattice is indeed at least a local minimum for potential function (28). All branches except one between the Γ and X points show a high deformation energy. In addition, the low energy $\Gamma - X$ branch contains shear deformations modes, which are less energetic than compression deformations for isotropic pair potentials, since they only slightly modify interparticle distances.

Figure 6 presents the lattice sums of the triangular, square, and honeycomb crystals for different number densities. The lattice sum for a given particle configuration C, in which each particle is equivalent to all others, is defined as the sum of the potential interaction energies between one of the particles p and all the others. Twice the energy per particle, u, is a generalization of the lattice sums that is well-defined for any configuration, including those for which particles are not equivalent.

At $\rho^{-1} = 1$, the value of u for the square, triangular, and honeycomb crystal configurations is 4.4556, 4.7635, and 5.2363, respectively. It is worthwhile to note that the honeycomb crystal u never comes close to the square lattice u, and thus can be discarded from the analysis. Over

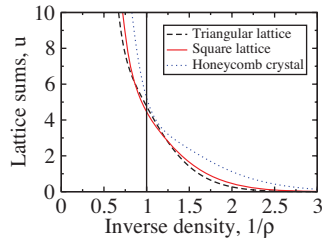

FIG. 6. Lattice sums in term of the inverse number density for the potential function (28). The black vertical line shows the number density ($\rho^{-1} = 1$) at which the optimization is conducted.

the $\rho^{-1} \in [0.9, 1.2]$ range, the square lattice has a lower energy than the triangular lattice. However, outside the $\rho^{-1} \in [0.91, 1.04]$ range, simulated annealing calculations produce configurations with lower energy than the square lattice. At $\rho^{-1} < 0.91$, a deformed triangular lattice becomes the ground state; while at $\rho^{-1} > 1.04$, a rectangular lattice is the ground state. In the case of the rectangular lattice, its nearest neighbor distance stays close to $r = 1$. This is due to the near linear dependence of the potential for values of r slightly greater than one (as the second derivative nearly vanishes). For such potentials, u decreases linearly with the sum of the distances of the four nearest neighbors, which is larger for a rectangular lattice than for a square lattice with an equal number density. Furthermore, rectangular lattices have farther third nearest neighbors than the corresponding second nearest neighbors of the square lattice.

While the positivity of the phonon spectrum ensures that the square lattice is stable under local deformations, it does not lead to any insight as to how potential (28) succeeds in stabilizing it. Alternatively, we can look at how u is affected when the square lattice is sheared, which is equivalent to the phonon modes near the Γ-point. The lattices obtained by the two independent shear modes are the rectangular lattice, with basis vectors $(1 + \varepsilon, 0)$ and $(0, (1 + \varepsilon)^{-1})$, and the rhomboidal lattice, with basis vectors $(1, \varepsilon)$ and $(0, 1)$. For the rectangular lattice,

$$\begin{aligned} u_{\text{rect}}(\varepsilon) &= u_{\text{square}} + [4v'(1) + 8\sqrt{2}v'(\sqrt{2}) + 4v''(1)]\varepsilon^2 + O(\varepsilon^3) \\ &= u_{\text{square}} + [4(-2.943) + 8\sqrt{2}(-0.917) \\ &\quad + 4(10.640)]\varepsilon^2 + O(\varepsilon^3) \\ &= u_{\text{square}} + 20.407\varepsilon^2 + O(\varepsilon^3), \end{aligned} \tag{34}$$

and for the rhomboidal lattice,

$$\begin{aligned} u_{\text{rect}}(\varepsilon) &= u_{\text{square}} + [2v'(1) + \sqrt{2}v'(\sqrt{2}) + 2v''(\sqrt{2})]\varepsilon^2 + O(\varepsilon^3) \\ &= u_{\text{square}} + [2(-2.943) + \sqrt{2}(-0.917) \\ &\quad + 2(5.702)]\varepsilon^2 + O(\varepsilon^3) \\ &= u_{\text{square}} + 4.220\varepsilon^2 + O(\varepsilon^3). \end{aligned} \tag{35}$$

We now clearly see that the monotonicity condition, which forces the first derivative to always be negative, requires the second-derivative to be large at both the first and second neighbors in order to achieve stability, since each appears in only one of the shear modes. An additional benefit of this analysis is that it explains how the square lattice is stable for a nonzero number density range; since both the first and second derivatives of potential (28) are continuous, the nearest-neighbor distance has to be modified by a positive amount before the $O(\varepsilon^2)$ terms in the shearing mode energies become negative (note: due to its symmetry, the $O(\varepsilon)$ term is always zero for the square lattice).

3. Point defects

While looking for the ground state of the potential function (28), we do not always obtain the actual ground state shown in Fig. 2. When an insufficiently slow annealing is

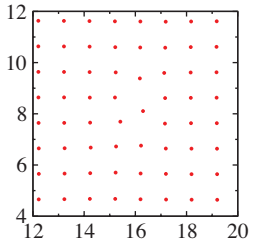

FIG. 7. Sample monovacancy defect on a 399-particle system (only a part of which is shown) with $\rho = 1$ for the potential function (28).

applied to the system, the end result often contains defects. Among these are polycrystalline configurations, where line defects show up at the boundaries between grains. However, some localized defects also arise. Such defects are caused by the presence (or absence) of an extra particle in the lattice.

Simply removing (or adding) a particle in the square lattice ground state does not reveal the actual behavior of such point defects. The presence of a defect locally deforms the lattice, which is necessary to minimize its energy. Starting with a square lattice to which a particle is either added or removed (while changing the lattice spacing to keep the overall number density constant at $\rho = 1$), the configuration is then relaxed using simulated annealing. The simulated annealing temperature is chosen to be low enough so that the lattice is not destroyed by melting and high enough so that the location of the defect can move through the lattice.

Figure 7 shows a mechanically stable structure for a monovacancy point defect, with a total energy difference of 0.62425 between the configuration with a single defect and the perfect square lattice. Figure 8 presents the interstitial defect, with an energy difference of 0.39646. These results are computed using modified 20×20 lattices, with 399 and 401 particles, respectively, but larger systems give essentially the same numbers. Starting with multiple defects also gives consistent results, although vacancies tend to attract each other. These single-defect numbers need to be compared with twice the energy per particle of the square lattice: $u = 4.45561$. It should be noted that there is no particular significance of which defect is the most energetic, since calculations with a similar potential (but with a larger cutoff R) find the interstitial defect to be the more energetic of the two.

An unexpected result is the complete absence of symmetry of the vacancy point defect configuration in Fig. 7. The results of 100 slow annealing simulations confirm that the configuration shown in Fig. 7 is indeed the stable configuration containing a monovacancy. Out of these, the system converges to a configuration of the type shown in Fig. 7, 69 times. In all of the 31 other cases, the system reaches a single type of alternative defect configuration. That other configuration has a defect energy of 0.63223, only 0.00798 higher than the lowest one. It is also more symmetrical, since it possesses a single axis of symmetry. The failure to find any other configuration than these two, especially one with lower energy, is compelling evidence that the configuration shown in Fig. 7 is indeed the lowest-energy-vacancy defect for this potential, even if it is asymmetric.

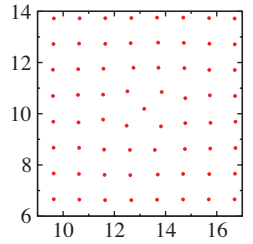

FIG. 8. Sample interstitial defect on a 401-particle system (only a part of which is shown) with $\rho = 1$ for the potential function (28).

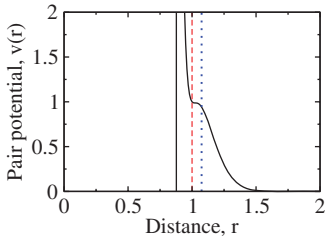

FIG. 9. Optimized monotonic nonconvex pair potential, targeting the square lattice at unit number density. The three vertical lines represent the nearest-neighbor distances for the honeycomb crystal (black solid), the square lattice (red dashed), and the triangular lattice (blue dotted), at the same number density. The value of $v(r)$ at these distances is 14.4371, 1 and 0.9428, respectively.

4. Dropping the convexity condition

It is possible to achieve the square-lattice ground state without the convexity constraint, keeping only the monotonicity requirement. Figure 9 depicts such an optimized potential. Since the potential presented in Fig. 9 has a short-range cutoff radial distance $r = R = 2$, u only depends on the first few coordination shells. Similar to the analysis in Sec. III A 1, we can explicitly write u for the square, triangular, and honeycomb crystals at unit density as

$$u_{\mathrm{SQ}} = 4v(r = 1) + 4v(r = 1.414) = 4.1611, \quad (36)$$

$$u_{\mathrm{TR}} = 6v(r = 1.075) + 6v(r = 1.861) = 5.6571, \quad (37)$$

$$u_{\mathrm{HC}} = 3v(r = 0.877) + 6v(r = 1.520) + 3v(r = 1.755) = 43.3517. \quad (38)$$

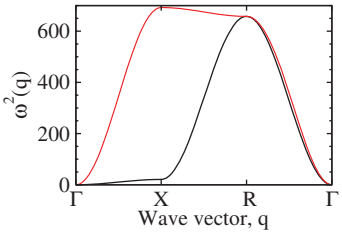

FIG. 10. Phonon spectrum for the potential shown in Fig. 9 on a square lattice with unit nearest neighbor distance ($\rho = 1$). Only a representative subset of wave vectors is presented here, but all the wave vectors have been tested to confirm that no mode is unstable.

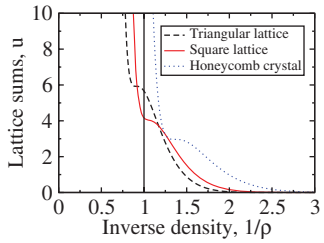

FIG. 11. Lattice sums in term of the inverse number density for the potential shown in Fig. 9. The vertical black line shows the number density ($\rho^{-1} = 1$) at which the optimization is conducted.

Again, since the Fig. 9 potential decreases steeply, almost all of the energy contributions stem from the nearest neighbors. For instance, the value of the potential at the square lattice second nearest neighbors is only $v(r = 1.414) = 0.0403$, which is much lower than its value at the nearest neighbors $v(r = 1) = 1$. While $v(r)$ is very low close to the second square neighbor, it is mostly constant between the square and triangular lattices nearest neighbors, only going down to $v(r = 1.075) = 0.9428$ at the triangular lattice nearest neighbors. This fact, combined with the higher nearest-neighbor coordination number of the triangular lattice (six versus the four for the square lattice), explains why the total energy of the triangular lattice is significantly higher than the total energy of the square lattice. In summary, removing the convexity requirement increases the set of possible potential functions that stabilize the square lattice. This is additional evidence that there exists a large family of monotonic potentials that stabilize the square lattice.

There are two important weaknesses of the method used to obtain the optimized potential. While intuition predicts that removing restrictions should result in a "better" potential, the phonon spectrum (Fig. 10) and the lattice sums (Fig. 11) indicate a ground state that is less stable than the monotonic convex potential (compare Figs. 5 and 6). This behavior occurs because for the Fig. 9 potential, only the triangular lattice is considered a competitor, and the optimizer simply tries to maximize the energy difference between both lattices at a single number density. This is done at the expense of the stability of the lattice, represented by number density variations (lattice sums) and local fluctuations (the phonon spectrum).

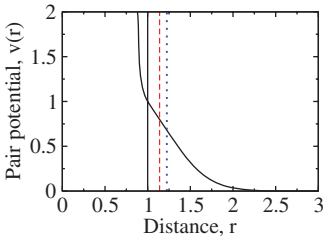

FIG. 12. Optimized convex pair potential function (39), targeting the honeycomb crystal at $\rho = 4/3\sqrt{3}$. The three vertical lines represent the nearest-neighbor distances for the honeycomb crystal (black solid), the square lattice (red dashed) and the triangular lattice (blue dotted), at $\rho = 4/3\sqrt{3}$. The value of $v(r)$ at these distances is 1, 0.7990 and 0.6795, respectively.

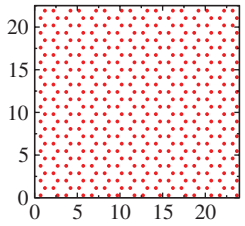

FIG. 13. The ground state of the potential function (39) with 416 particles in a $24\times13\sqrt{3}$ box with periodic boundary conditions, obtained by slowly annealing the system from a fluid.

B. Honeycomb crystal

As with the square lattice, we also use our method to obtain a pair potential for the honeycomb crystal with a nearest neighbor distance of unity ($\rho = 4/3\sqrt{3}$). The optimization is restricted to monotonic convex potentials with a cutoff at $r = 3$. While intuition leads one to believe that the presence of the square lattice in the competitor set **C** is required to find an optimized potential for which the ground state is the honeycomb lattice, this is not the case, since a set **C** consisting only of the triangular lattice is sufficient to obtain a potential with the desired ground state. The resulting optimized potential is

$$v(r) = \begin{cases} \left(\dfrac{3.767}{r} - \dfrac{48.246}{r^2} + \dfrac{230.514}{r^3} \right. \\ -\dfrac{451.639}{r^4} + \dfrac{56.427}{r^5} + \dfrac{1000}{r^6} \\ -\dfrac{868.468}{r^7} - \dfrac{776.495}{r^8} + \dfrac{1000}{r^9} \\ \left. +\dfrac{521.638}{r^{10}} - \dfrac{1000}{r^{11}} + \dfrac{333.502}{r^{12}}\right) & r \le 3, \\ 0 & r > 3. \end{cases} \tag{39}$$

This function is plotted in Fig. 12. Figure 13 shows the ground-state configuration of potential (39), obtained using simulated annealing down to zero temperature, starting with a random arrangement of particles generated by a Poisson point process. Whether the ground state is reached for a given simulation depends greatly on the orientation the crystal takes during cooling. Due to the boundary conditions, only two orientations allow the honeycomb crystal to be formed without defects, which makes reaching the ground state difficult. However, when the crystal is not oriented correctly, the resulting configuration is still visibly a honeycomb crystal, albeit with

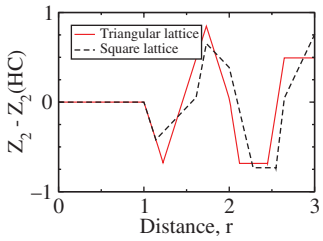

FIG. 14. Differences between the coordination functions of second order $\mathcal{Z}_2$ of the triangular and square lattices and the honeycomb crystal. All three crystal have a number density of $4/3\sqrt{3}$.

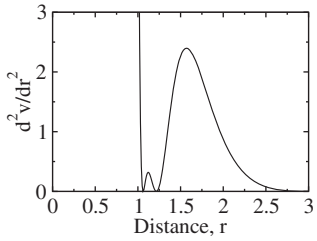

FIG. 15. Second derivative of the pair potential d^2v/dr^2 from Eq. (39) versus the distance r.

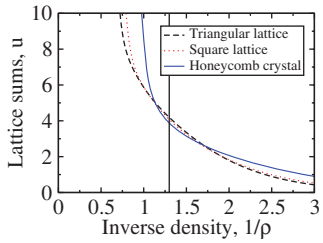

FIG. 17. Lattice sums in term of the inverse number density for potential (39). The vertical black line shows the number density ($\rho^{-1} = 3\sqrt{3}/4$) at which the optimization is conducted.

minor defects and deformation, as well as a higher energy than the perfect honeycomb crystal configuration. During the ground state simulations, no other configuration is found to have a lower energy than the honeycomb crystal. Out of the four slowest simulated-annealing calculations executed with this potential, two of them reach the perfect honeycomb crystal. The two others do not align correctly with the boundary conditions and thus converge to honeycomb crystals with a slight shear and some localized defects.

As with the square-lattice potential, we conduct simulated-annealing calculations with variable periodic-box dimensions. For boxes of constant area, all converged configurations have higher energy than the honeycomb crystal reinforcing our conclusion that potential (39) has the honeycomb-crystal configuration as its ground state.

1. Discrimination against other crystals

Since we are using a pair potential with a short-ranged cutoff, the value of twice the energy per particle u only depends on the first few coordination shells. At $\rho = 4/3\sqrt{3}$, we can explicitly write u for the honeycomb, triangular, and square crystals:

$$u_{\mathrm{HC}} = 3v(r=1) + 6v(r=1.732) + 3v(r=2) + 6v(r=2.646) = 3.8812, \quad (40)$$

$$u_{\mathrm{TR}} = 6v(r=1.225) + 6v(r=2.121) + 12v(r=2.449) = 4.1919, \quad (41)$$

$$u_{\mathrm{SQ}} = 4v(r=1.140) + 4v(r=1.612) + 4v(r=2.280) + 8v(r=2.649) = 4.0755. \quad (42)$$

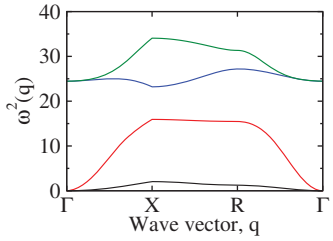

FIG. 16. Phonon spectrum for potential (39) on a honeycomb crystal with unit nearest neighbor distance ($\rho = 4/3\sqrt{3}$). Only a representative subset of wave vectors is presented here, but all wave vectors have been tested to confirm that no mode is unstable.

That potential (39) succeeds in having a lower u for the honeycomb crystal than the triangular lattice is readily explained by the observation that the triangular-lattice coordination number is twice that of the honeycomb crystal. The triangular-lattice nearest neighbors have an interaction energy of $v(r = 1.225) = 0.6795$, which is much higher than half of the honeycomb-crystal nearest-neighbors interaction [$v(r = 1) = 1$]. The square lattice also has a larger coordination number than the honeycomb crystal, with a value equivalent to four-thirds of the latter. The square-lattice nearest neighbors have an interaction energy slightly larger than three-fourths of the honeycomb-crystal nearest neighbors [$v(r = 1.140) = 0.7990$ versus $v(r = 1) = 1$]. This energy difference is further supplemented by the second-nearest neighbors of the square lattice, which are closer than those of the honeycomb crystal. Even if they are less numerous (four instead of six), their interaction energy is much larger [$v(r = 1.612) = 0.2123$ versus $v(r = 1.732) = 0.1292$].

As with the square lattice, the coordination function of second order $\mathcal{Z}_2$ can be used to determine which features are required in a potential's second derivative if the potential is to have the honeycomb crystal as its ground state. Figure 14 shows the differences in $\mathcal{Z}_2$ between the honeycomb crystal and its two main competitors, the triangular and the square lattices. In this figure, we see that after the quasi-hard-core repulsion region ($r < 1$), the second derivative must be close to zero up to $r \sim 1.5$, before becoming large up to $r \sim 2$, in order for the triangular and square lattices to be energetically unfavorable relative to the honeycomb crystal. This behavior can be observed in the second derivative of the proposed potential (Fig. 15). The reason the second derivative has two distinct r values at which it goes down to zero is a consequence of the potential-function form restrictions, which does not allow a wide well without adding another minimum.

As with the square lattice, we use the information extracted from $\mathcal{Z}_2$ to build a piecewise-polynomial potential for

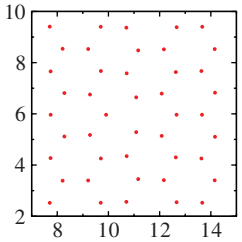

FIG. 18. Sample monovacancy defect on a 415 particles system (only part of which is shown) with $\rho = 4/3\sqrt{3}$ for the potential function (39).

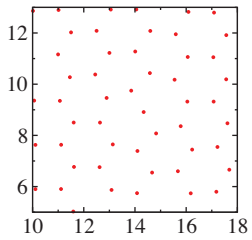

FIG. 19. Sample interstitial defect on a 417 particles system (only a part of which is shown) with $\rho = 4/3\sqrt{3}$ for the potential function (39).

which the honeycomb crystal is the ground state,

$$v(r) = \begin{cases} 5r^2 - 10.5r + 5.875 & r \le 1, \\ -0.5r + 0.875 & 1 < r \le 1.5, \\ 0.5r^2 - 2r + 2 & 1.5 < r \le 2, \\ 0 & 2 < r, \end{cases} \tag{43}$$

with a second derivative

$$\frac{d^2v}{dr^2} = \begin{cases} 10 & r \le 1, \\ 0 & 1 < r \le 1.5, \\ 1 & 1.5 < r \le 2, \\ 0 & 2 < r. \end{cases} \tag{44}$$

Simulated annealing calculations show that the ground state of potential (43) is indeed the honeycomb crystal. However, as is the case for the square lattice equivalent potential [cf. Eq. (32)], some caveats apply; mainly the discontinuity of the second derivative at $r = 1$ prevents the verification of the honeycomb crystal stability by its phonon spectrum.

2. Stability

As for the case of the square lattice, three properties must be checked to determine whether the proposed potential forms a stable honeycomb crystal: is the honeycomb crystal the ground state over a nonvanishing number density range, are the phonon modes stable, and what are the effects of perturbing the potential form? Again, only the first two of these are appraised in this paper.

Figure 16 shows the squared frequency of the different phonon modes as a function of their wave vector. An exhaustive search confirms that there is no mode for which the squared frequency is negative indicating that the honeycomb crystal is at least a local minimum in the energy landscape for the pair potential function (39).

Figure 17 compares the lattice sums u at different number densities for the triangular, square, and honeycomb crystals. At $\rho^{-1} = 3\sqrt{3}/4$, the u for the honeycomb, triangular, and square crystals are equal to 3.8812, 4.1919, and 4.0755, respectively. For $\rho^{-1} \in [1.15, 1.6]$, the honeycomb crystal has a lower energy than both the square and the triangular lattices. This range is further refined to $\rho^{-1} \in [1.2, 1.4]$, where simulated annealing calculations produce configurations recognizable as the honeycomb crystal as the ground state. However, many of these configurations are not actually the honeycomb crystal, but rather deformed versions of it. By calculating the phonon spectrum of the honeycomb crystal over this range, we determine that the honeycomb crystal is only stable over $\rho^{-1} \in [1.25, 1.35]$. At larger densities ($\rho^{-1} < 1.2$), the potential favors a configuration consisting of pentagonal rings (compared to the hexagonal rings of the honeycomb crystal), while at lower densities ($\rho^{-1} > 1.4$), the potential favors particles in evenly spaced chains, effectively reducing the number of nearest neighbors to only two.

Similar to the square lattice, we can explore the effect of shearing on the honeycomb crystal to understand how potential (39) stabilizes it against local deformations. Unlike the square lattice, which has two independent shear modes, both of the honeycomb crystal modes have equal energy up to a constant, so we only need to verify one of them. Looking at the crystal obtained by stretching the honeycomb crystal by $(1+\varepsilon)$ in the x-direction and $(1+\varepsilon)^{-1}$ in the y-direction, we obtain

$$\begin{aligned} u_{\text{stretched}}(\varepsilon) &= u_{\text{HC}} + \left[\begin{array}{l} \frac{9}{2}v'(1) + 9\sqrt{3}v'(\sqrt{3}) + 9v'(2) + 9\sqrt{7}v'(\sqrt{7}) \\ +\frac{3}{2}v''(1) + 9v''(\sqrt{3}) + 6v''(2) + 21v''(\sqrt{3}) \end{array} \right] \varepsilon^2 + O(\varepsilon^3), \\ &= u_{\text{HC}} + \left[\begin{array}{l} \frac{9}{2}(-1.561) + 9\sqrt{3}(-0.564) + 9(-0.189) + 9\sqrt{7}(-0.003) \\ +\frac{3}{2}(8.882) + 9(1.971) + 6(0.873) + 21(0.0280) \end{array} \right] \varepsilon^2 + O(\varepsilon^3), \\ &= u_{\text{HC}} + 19.303\varepsilon^2 + O(\varepsilon^3). \end{aligned} \tag{45}$$

Again, as in the square lattice case, large second-derivative values for a monotonic potential are necessary to stabilize the honeycomb crystal.

3. Point defects

As for the potential with a square lattice ground state, it is also relevant to study the behavior of point defects for the

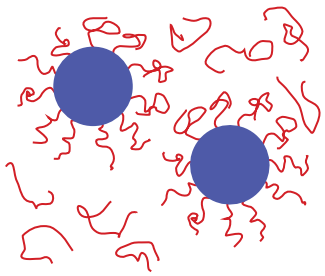

FIG. 20. Sketch of possible colloids with a pair potential similar to those from Eqs. (28) and (39). The hard-core colloids are covered with attached repelling polymers, whose average extension is controlled by the dissolved polymer chains.

potential with a honeycomb ground state. Figure 18 shows the monovacancy defect, which has an energy of 0.28414, while Fig. 19 shows the interstitial defect, which has an energy of 0.44761. Similar to the square lattice, there is no fundamental reason for why the vacancy is less energetic than the interstitial defect.

IV. CONCLUSIONS AND DISCUSSION

The possibility of designing pair potentials that result in the self-assembly of unusual targeted many-particle configurations is not surprising if one allows for one or a few potential wells at strategic locations.[10,12] Whether it is possible to find potentials that stabilize novel classical ground states in Euclidean space without any wells is not at all obvious. In this paper, we have shown that potentials without wells, namely, monotonic convex repulsive pair interactions, can produce low-coordinated ground states in $\mathbb{R}^2$ such as the square lattice and the honeycomb crystal. Indeed, our work demonstrates that there exists a large family of monotonic potentials that stabilize the square and honeycomb crystals.

Lindenblatt *et al.*[18] have fabricated the so-called "hairy colloids" (see Fig. 20). These colloids are formed by grafting polymer chains onto the surface of nanoscopic microgel spheres in a matrix of polymer chains. The swelling of the grafted chains can be controlled by varying the molecular weight of the matrix chains, going from "wet brushes," with a lot of swelling for short matrix chains, to "dry brushes," with little swelling for long matrix chains. The coronas of the grafted polymers avoid each other, giving rise to a short-range repulsive effective pair potential between the resulting colloids. Together with a hard-core repulsion when the microgel spheres touch, these colloid interactions offer promise of being similar to Eqs. (28) and (39), although experimental realization remains an unfulfilled endeavor.

However, there is no evidence that the pair potentials of these "hairy colloids" have a strong dip in their second derivative, a feature is crucial for the self-assembly of both the square lattice and the honeycomb crystal. Instead of trying to synthesize colloids with potentials identical to those presented in this paper, another approach would be to determine what monotonic repulsive potentials are possible using grafted polymers of variable length. If the resulting potentials can be written in the form of $v(r) = \int_s ds c(s) f(r,s)$, then the generalized coordination function formalism from Sec. II C could be used to explore which length distribution of grafted polymers should be used for the colloids to self-assemble in targeted configurations.

We reiterate that we have shown there are monotonic convex potentials with low-coordinated ground states in two-dimensional Euclidean spaces. While it has been suggested that such potentials exist in three dimensions,[2,9,24] phonon spectra were not computed in these studies. An interesting area for further research would be to verify whether the generalized-coordination-function techniques introduced in this paper can be extended to optimize monotonic convex potentials to stabilize low-coordinated three-dimensional crystal ground states, such as the simple cubic and diamond crystals. Another topic that warrants further research is whether purely repulsive interactions can be achieved in the laboratory to yield low-coordinated ground-state configurations.

ACKNOWLEDGMENTS

This research was supported by the U.S. Department of Energy, Office of Basic Energy Sciences, Division of Materials Sciences and Engineering under Award DE-FG02-04-ER46108. We also acknowledge support from the Natural Sciences and Engineering Research Council of Canada.

[1] G. M. Whitesides, J. P. Mathias, and C. T. Seto, Science **254**, 1312 (1991).
[2] M. Watzlawek, C. N. Likos, and H. Löwen, Phys. Rev. Lett. **82**, 5289 (1999).
[3] D. Gottwald, C. N. Likos, G. Kahl, and H. Löwen, Phys. Rev. Lett. **92**, 68301 (2004).
[4] S. A. Jenekhe and X. L. Chen, Science **283**, 372 (1999).
[5] A. M. Jackson, J. W. Myerson, and F. Stellacci, Nat. Mater. **3**, 330 (2004).
[6] M.-P. Valignat, O. Theodoly, J. C. Crocker, W. B. Russel, and P. M. Chaikin, Proc. Natl. Acad. Sci. U.S.A. **102**, 4225 (2005).
[7] A.-P. Hynninen, C. G. Christova, R. Van Roij, A. Van Blaaderen, and M. Dijkstra, Phys. Rev. Lett. **96**, 138308 (2006).
[8] C. N. Likos, B. M. Mladek, A. J. Moreno, D. Gottwald, and G. Kahl, Comput. Phys. Commun. **179**, 71 (2008).
[9] S. Prestipino, F. Saija, and G. Malescio, Soft Matter **5**, 2795 (2009).
[10] M. C. Rechtsman, F. H. Stillinger, and S. Torquato, Phys. Rev. E **73**, 011406 (2006).
[11] M. C. Rechtsman, F. H. Stillinger, and S. Torquato, Phys. Rev. E **74**, 021404 (2006).
[12] M. C. Rechtsman, F. H. Stillinger, and S. Torquato, Phys. Rev. E **75**, 031403 (2007).
[13] M. C. Rechtsman, F. H. Stillinger, and S. Torquato, J. Phys. Chem. A **111**, 12816 (2007).
[14] M. C. Rechtsman, F. H. Stillinger, and S. Torquato, Phys. Rev. Lett. **101**, 085501 (2008).
[15] O. U. Uche, S. Torquato and F. H. Stillinger, Phys. Rev. E **74**, 031104 (2006).
[16] R. D. Batten, F. H. Stillinger, and S. Torquato, J. Appl. Phys. **104**, 033504 (2008).
[17] M. Florescu, S. Torquato, and P. J. Steinhardt, Proc. Natl. Acad. Sci. U.S.A. **106**, 20658 (2009).
[18] G. Lindenblatt, W. Schärtl, T. Pakula, and M. Schmidt, Macromolecules **34**, 1730 (2001).
[19] V. N. Manoharan, M. T. Elsesser, and D. J. Pine, Science **301**, 483 (2003).
[20] S. Torquato, Soft Matter **5**, 1157 (2009).
[21] H. Cohn and A. Kumar, Proc. Natl. Acad. Sci. U.S.A. **106**, 9570 (2009).
[22] É. Marcotte, F. H.Stillinger, and S. Torquato, Soft Matter **7**, 2332 (2011).
[23] Of course, rigorously proving that a given configuration is a true ground state is highly nontrivial, so we must accept the results from carefully designed numerical methods.
[24] Unlike Ref. 2 which attempts to find minimum free-energy configurations at positive temperatures, Ref. 9 bases its claims only on lattice sums for a limited number of possible crystal configurations.